Journal of the Serbian Society for Computational Mechanics / Vol. 17 / No. 2, 2023 / pp 69-86
(10.24874/jsscm.2023.17.02.06)

PREDICTION OF DRAG AERODYNAMIC COEFFICIENT OF THE 155MM PROJECTILE UNDER AXISYMMETRIC FLOW USING DIFFERENT APPROACHES

Abdellah Ferfouri[1*], Toufik Allouche[1], Damir D. Jerković[1], Nebojša Hristov[1], Milan Vučković[2] and Abdeselem Benmeddah[1]

[1] University of Defence – Military Academy, Veljka Lukića Kurjaka 33, 11042 Belgrade, Serbia
e-mail: fer-abdel@hotmail.com, toufik.allouche@gmail.com, damir.jerkovic@va.mod.gov.rs, nebojsahristov@gmail.com, benabde1993@gmail.com
[2] Military Technical Institute, Ratka Resanovića 1, 11000 Belgrade, Serbia
e-mail: milvuk.kg@gmail.com
**Corresponding author*

Abstract

The determination of the total aerodynamic load which negatively influences the movement of artillery projectiles is inevitable and indispensable in order to be able to increase or control their ranges. The main part of this aerodynamic load that has the most influence on projectile movement is the drag force, which acts in the opposite direction to the velocity vector and therefore opposes its movement. From this, in this present work, the total drag coefficient of the 155mm M107 axisymmetric projectile under axisymmetric flow, at zero yaw, was predicted by semi-empirical and computational fluid dynamics (CFD) approaches in the three flow regimes, also the influence of its components on the total drag was analysed. The average deviation of the total drag coefficient in the three flow regimes, compared to the reference experimental results, is 5.7% for the semi-empirical results and 1.7% for the computational results. Analysis of the influence of the total drag components, such as pressure drag, friction drag and base drag, permitted to calculate their influence rates on the total drag as a function of Mach number and flow regime.

Keywords: drag aerodynamic coefficient, drag components, computational fluid dynamics, axisymmetric projectile.

1. Introduction

Modern ballistics can be categorized into three distinct disciplines: internal ballistics, external ballistics and terminal ballistics, which describe, respectively, the propulsion, atmospheric flight and target impact action of projectile (McCoy. 1998). The modern science of external ballistics has evolved as a specialized branch of the dynamics of rigid bodies moving under the influence of gravitational and aerodynamic forces (McCoy. 1998). The subject 'Aerodynamics' in ballistics refers to the study of air flow around a projectile or any other object of interest. A projectile is a rigid body that, during its trajectory towards the target, is under the influence of aerodynamic

forces and moments created by the action of the air passing through it. There are three research approaches in modern studies of aerodynamics. These are the experimental approach, the theoretical approach (analytical or semi-analytical) and the computational fluid dynamics (CFD) approach. Each approach has its advantages and disadvantages. Usually, the most effective approach is to combine experimental and theoretical/CFD research in the most rational way to solve a particular problem (Roy. 2012).

Theoretical and computational fluid dynamics (CFD) studies have provided valuable insights into a wide range of flow problems to date. However, these approaches also have their limitations. The primary limitation arises from the fact that the governing equation for real viscous compressible flow around an object, known as the Navier-Stokes equations, cannot generally be solved analytically (Roy. 2012). In principle, the Navier-Stokes equations can provide a comprehensive description of all flow regimes relevant to aerodynamics. However, achieving this requires highly accurate numerical solutions of the governing equations, considering appropriate initial and boundary conditions. The only two devices available to nature to communicate with an object moving through the air are the pressure which normally acts on its surface; and the shear stress distribution on its surface which acts tangentially to it. Hence, the main objective of aerodynamics is to determine the distribution of pressure and shear stress around the object and to integrate their distribution in order to obtain the resultant force and moment acting on the object. In general, the resultant force and moment acting on a moving rigid projectile can be resolved into three components each. The resultant force could be broken down into drag, side and normal forces, and the resultant moment could be separated into roll moment, pitch moment and yaw moment. Most forces and moments are expressed as dimensionless coefficients. The accuracy and control in flight of a projectile is partly conditioned by the knowledge of the aerodynamic coefficients associated with each force and moment acting on it. The main part of the total aerodynamic load, in free flight, which has the most influence on the trajectory range is the drag force, which acts in the opposite direction to the velocity vector. It is the force that opposes the motion of the projectile.

Research continues to this day on 155mm projectiles which is a NATO-standard artillery caliber that is used in many field guns, howitzers, and gun-howitzers. Chang et al. (2023) studied the aerodynamic coefficients of a 155mm spin-stabilized projectile, controlled by a microspoiler, using a computational fluid dynamics (CFD) simulation that has been validated by the current literature and a wind-tunnel test. Paul et al. (2023) realized numerically (CFD) and experimentally a passive method in order to reduce the base drag of a 155mm projectile using the inward turning base-bleed technique. Szklarski et al. (2020) carried out an impact point prediction guidance parametric study for 155 mm rocket assisted artillery projectile with lateral thrusters in which the aerodynamic coefficients were calculated using semi-empirical engineering-level codes and analytical methods. Serdarevic-Kadic et al. (2019) carried out numerical simulations of the airflow around a 155 mm arbitrary projectile in order to determine the effects of the base shape on the total drag. DeSpirito (2017) performed a CFD aerodynamic characterization of 155mm spin-stabilized projectile at high angles of attack. Fonte-Boa et al. (2017) proposed a geometry for a 155 mm firefighting projectile taking that of the 155 mm M107 projectile as a starting geometry in which the finite volume code STAR - CCM+ is used to calculate forces and moments acting on the projectile.

As for this present work, it aims to predict the total drag coefficient of the 155mm M107 axisymmetric projectile under axisymmetric flow, at zero-yaw, by semi-empirical and numerical (CFD) calculations in an interval of Mach numbers including the three regimes of flow, as well as to analyse the influence of drag components, such as pressure drag, friction drag and vortex drag (base drag) on the total drag. This paper is divided into five parts: the second part describes the aerodynamic model of the projectile and calculation methods, the third and fourth parts

describes the calculation results and their analysis and discussion, and finally, the fifth part contains the main conclusions.

2. Aerodynamic model of the projectile

During the motion of the projectile through the air, the axis of the projectile makes a certain angle σ with the velocity vector $\vec{V}_\infty$, which is called the angle of attack. In such a case, the total aerodynamic force $\vec{R}$ does not act in the direction of the projectile's velocity or axis. Its effect is not in the center of gravity CM but in some point, CP called the center of pressure (Fig.1) (Viličić & Gajić, 1979).

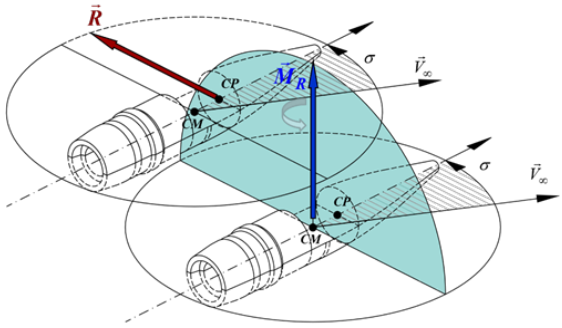

Fig. 1. Aerodynamic force and moment

The aerodynamic forces acting on the projectile in the center of pressure is (Fig.2):

$$R = \begin{bmatrix} X \\ \overline{Y} \\ \overline{Z} \end{bmatrix} = q_\infty S \begin{bmatrix} C_X \\ C_{\overline{Y}} \\ C_{\overline{Z}} \end{bmatrix} \tag{1}$$

The aerodynamic moment acting on the projectile is (Fig.2):

$$M_R = \begin{bmatrix} L \\ \overline{M} \\ \overline{N} \end{bmatrix} = q_\infty S d \begin{bmatrix} C_L \\ C_{\overline{M}} \\ C_{\overline{N}} \end{bmatrix} \tag{2}$$

Where are: $q_\infty = \rho V_\infty^2/2$ dynamic pressure, $S = \pi d^2/4$ – reference cross-section, d – projectile reference diameter, $C_X, C_{\overline{Y}}, C_{\overline{Z}}$ – aerodynamic coefficients of aerodynamic forces, $C_L, C_{\overline{M}}, C_{\overline{N}}$ – aerodynamic coefficients of aerodynamic moments, ρ – air density, $\vec{V}_\infty$ – velocity vector.

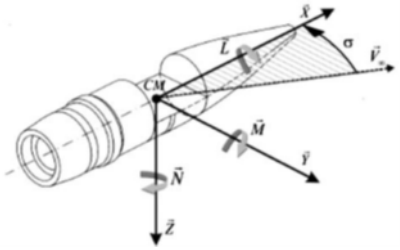

Fig. 2. Aerodynamic force and moment with components

Components of aerodynamic force and moment are: $\underline{X}$ – axial force, $\overline{Y}$ – side force, $\overline{Z}$ – normal force, L – roll moment, $\overline{M}$ – pitch moment, N – yaw moment. The aerodynamic coefficient of the axial force $\vec{X}$ is denoted by C_X. The axial force is in the opposite direction from the longitudinal axis of the body coordinate system, that is, the value of the coefficient is negative. The dependence of the coefficient on the angle of attack $C_X(-\sigma) = C_X(\sigma)$ can be represented by (Regodić, 2006):

$$C_X = C_{X0}(M_a) + C_{X\sigma^2}(M_a)\sigma^2 \tag{3}$$

According to Regodić (2006), $C_{X\sigma^2} = \frac{1}{2}\left(\frac{\partial^2 C_X}{\partial \sigma^2}\right)$.

If the flow around the projectile is axisymmetric, which means that the longitudinal axis of symmetry of the projectile coincides with the velocity vector and the angle of attack σ is equal to zero, all aerodynamic coefficients are equal to zero except for the axial force coefficient which will be reduced to $C_X = C_{X0}(M_a)$ and depends on Mach number M_a and projectile shape. The aerodynamic coefficient of the axial force, i.e., the drag aerodynamic coefficient, under axisymmetric flow results from three influential factors (Regodić et al. 2013): (1) pressure drag, (2) friction drag and (3) vortex drag (base drag). It is analytically presented as the sum of three parts of the coefficient:

$$C_{D0} = C_{Dp} + C_{Df} + C_{Db} \tag{4}$$

The first term C_{Dp} is a consequence of the influence of normal pressure on the surface, due to the appearance of shock waves in the transonic and supersonic speed range, and is called the pressure drag coefficient which is composed of: pressure drag coefficient due to projectile head (nose) C_{D1}, pressure drag coefficient due to boattail C_{D3} and pressure drag coefficient due to a rotating band C_{D4}. The second term C_{Df} is due to air friction (viscosity) on the surface, and is called the friction drag coefficient. The third term is the base drag coefficient C_{Db} due to the negative pressure behind the base of the projectile and it mainly depends on the Mach number. According to the research (Regodić et al. 2013; Sivasubramanian et al. 2006; Sahu & Heavey, 1997) the base drag coefficient C_{Db} can represent on average up to 40% of the total drag coefficient.

2.1 Projectile model for calculation

The calculation of the flow and the total drag coefficient C_{D0} under axisymmetric flow i.e., at zero-yaw, was performed on the 155mm M107 classic axisymmetric projectile, shown in fig.3. The projectile is a rigid body with an axisymmetric shape without additional aerodynamic

surfaces and propulsion. The movement speed of the projectile is relatively high, up to several Mach numbers, which during the flight of the projectile decreases below the speed of sound. This allows the flow image to be visualized in all three flow regimes.

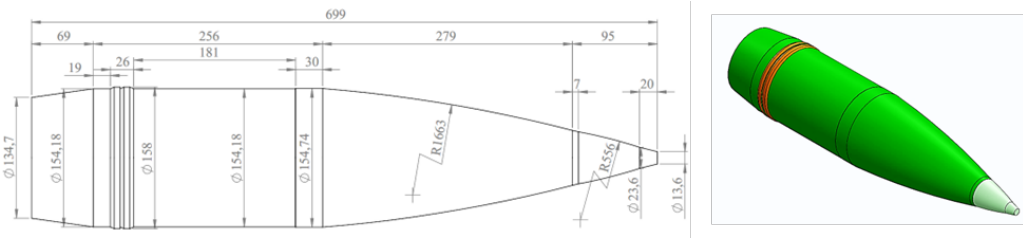

Fig. 3. 155mm M107 projectile model, dimensions (left) and 3D model (right)

The projectile model analysed in this work is based on the standard construction parameters of the existing 155mm M107 projectiles with characteristic parameters given in fig.3.

2.2 Calculation methods

As it was already mentioned, in this work the prediction of the total drag coefficient C_{D0} at zero-yaw is done by two methods of calculation, namely, semi-empirical and numerical (CFD).

2.2.1 Semi-empirical approach

The semi-empirical approach was carried out using the semi-empirical program solution AERODR of Regodić (2003) which is based on the computer program "MC DRAG" of McCoy (1981). AERODR determines the values of the total drag coefficient C_{D0} and its components (C_{D1}, C_{D3}, C_{D4}, C_{Db} and C_{Df}) according to the Mach number M_a in axisymmetric flow ($\sigma = 0$), whose input data (Table 1) are the dimensions that define the shape of the projectile as well as the position of its center of mass and the type of boundary layer. The semi-empirical program solution AERODR for aerodynamic calculation at zero-yaw was made in MATLAB programming languages.

Parameter	**Designation and Unit**	**Value**
Projectile reference diameter	$DREF[mm]$	155
Projectile length in calibers	$LT[cal]$	4,5097
Length of the front part in calibers	$LN[cal]$	2,4129
Ratio of the front ogive	$RTR[/]$	1
Tail cone length in calibers	$LBT[cals]$	0,445
Front diameter of fuse in calibers	$DM[cal]$	0,0877
Base diameter in calibers	$DB[cal]$	0,869
Rotating band diameter in calibers	$DBND[cal]$	1,01935
Position of the center of mass from the fuse in calibers	$XCGN[cal]$	2,9572
Boundary layer type (l/t – laminar = 1, t/t – turbulent = 2)	$BLC[/]$	1

Table 1. Input data of the semi-empirical approach

2.2.2 Computational approach

The Computational approach was carried out using CFD software. The governing equations are based on Reynolds Averaged Navier Stokes equations (RANS), given by equations for the conservation of mass (continuity), momentum and energy, presented below (Dali et al. 2019; Nicolás-Pérez et al. 2017; Belaidouni et al .2016). To achieve closure of the governance equations, the $k-\varepsilon$ realizable model was chosen in view of its wide use in similar studies (Chang et al. 2023; Aziz et al. 2020; Torangatti et al. 2014; Belaidouni et al. 2016), default constant values were employed for this model.

- Continuity

$$\frac{\partial \rho}{\partial t}+\frac{\partial(\rho u_i u_j)}{\partial x_i}=0 \tag{5}$$

- Momentum

$$\frac{\partial(\rho u_i)}{\partial t}+\frac{\partial(\rho u_i u_j)}{\partial x_j}=-\frac{\partial P}{\partial x_i}+\frac{\partial \tau_{ij}}{\partial x_i} \tag{6}$$

- Energy

$$\frac{\partial}{\partial t}\left[\rho(e+\frac{V^2}{2})\right]+\frac{\partial}{\partial x_j}\left[\rho u_i(e+\frac{V^2}{2})+P+q_j-u_i\tau_{ij}\right]=0 \tag{7}$$

In the previous equations, u denotes instantaneous velocity, V the velocity modulus, ρ the gas density, P the gas pressure, q_j the heat flux and τ_{ij} is the viscous shear tensor. In addition, the equation of state for an ideal gas is considered.

Numerical discretization of the flow domain is defined by the lower boundary of the numerical domain represented by the projectile model and the upper boundary defined at a sufficient distance from the projectile model, where the zone of undisturbed flow field is assumed. The construction of the mesh was carried out using the program for creating numerical mesh GAMBIT. As shown in fig.4, the limit of the calculation domain is 35D in the vertical extent, 30D in front of the projectile and 50 behind the projectile (where D denotes the diameter of the projectile). The structured mesh is composed of 100156 quadrilateral cells (343 cells were used on the projectile model) with y^+ from 0.7 to 4 on the walls of the projectile model. This mesh density was determined after testing several types of mesh density, shown in fig.5.

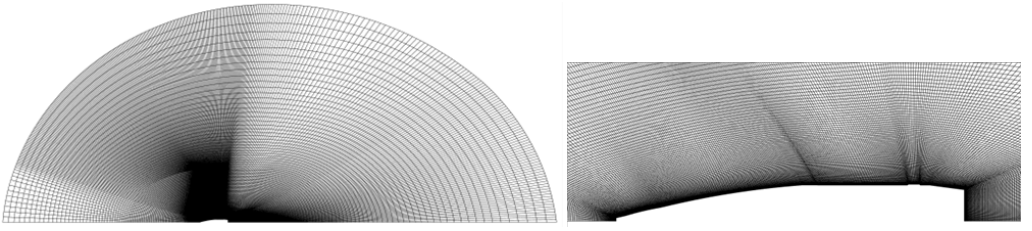

Fig. 4. View of the meshing domain (left) and mesh around the projectile model (right)

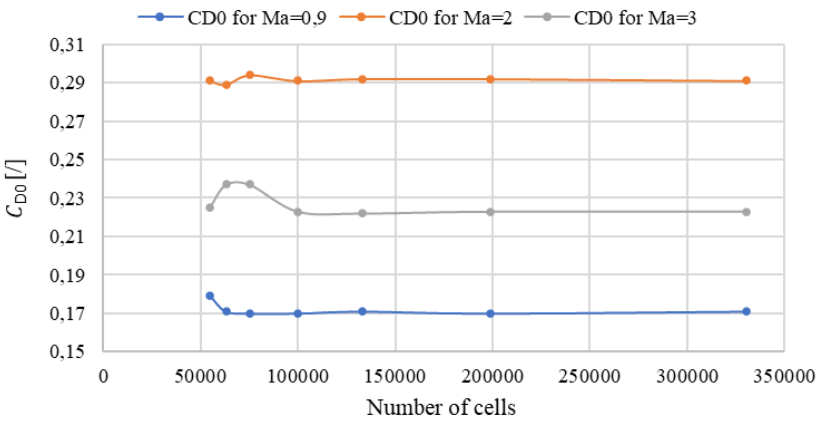

Fig. 5. Determining the independence of the mesh from the number of cells

The flow numerical calculation was performed by Ansys Fluent for the range of Mach numbers from 0.5 to 3, i.e., the three flow regimes. The calculation is based on the density solver, for the case of axisymmetric flow, and in it the density field is determined from the continuity equation, while the pressure field is determined from the state equation and the velocity field from the momentum equation, and in the considered analysis it was assumed that air is an ideal gas, with standard parameters according to the ICAO standard, with a viscosity coefficient based on Sutherland's law with three coefficients. Operating pressure has been set to $0Pa$. Three boundary conditions are used throughout the numerical domain: the far-field pressure boundary, the wall boundary, and the axisymmetric boundary. The axisymmetric boundary is applied to the longitudinal axis of the projectile. Air parameter data for different values of Mach numbers are given in table 2, for total parameters according to the ICAO atmosphere.

Mach number $M_a[/]$	Pressure $p[Pa]$	Temperature $T[K]$	Velocity $V_\infty[m/s]$	Density $\rho[kg/m^3]$
0,5	85.418,92	275,14	166,19	1,081569
0,6	79.439,20	269,50	197,39	1,026904
0,7	73.048,02	263,11	227,54	0,967219
0,8	66.471,39	256,12	256,56	0,904159
0,9	59.909,43	248,62	284,38	0,839485
0,95	56.687,28	244,73	297,81	0,806961
1	53.528,15	240,75	310,93	0,774586
1,1	47.455,99	232,61	336,19	0,710749
1,2	41.784,10	224,30	360,15	0,648986
1,5	27.601,24	199,24	424,29	0,482621
2	12.949,79	160,50	507,75	0,281088
2,5	5.930,32	128,40	567,68	0,160904
3	2.758,44	103,18	610,66	0,093137

Table 2. Values of atmospheric input parameters for computational approach

Air parameter data for different values of Mach numbers were calculated using the below equations, where the total parameters of the atmosphere were taken according to the ICAO atmosphere and that $p_0 = 101325Pa$ and $T_0 = 288{,}16K$.

$$p = p_0 \Big/ \left[1 + ((\kappa - 1)/2) M_a^2\right]^{\frac{\kappa}{\kappa - 1}} \tag{8}$$

$$T = T_0 \Big/ \left[1 + ((\kappa - 1)/2) M_a^2\right] \tag{9}$$

$$V_\infty = M_a \cdot a = M_a \sqrt{\kappa R T} \tag{10}$$

$$\rho = p / RT \tag{11}$$

Where are: $\kappa = 1,4\left[/\right]$ – specific heat ratio for air, $R = 287\left[J/kgK\right]$ – air specific constant and $a\left[m/s\right]$ speed of sound.

The implicit solution method was applied to calculate the flow parameters. A second-order discretization is chosen for pressure, momentum, energy and turbulence parameters such as turbulent kinetic energy and turbulent dissipation rate. The flow is calculated using the Roe-FDS scheme and the gradients are calculated based on the Green-Gauss node. The value of the Courant number was in relation to the number of iterations from 5 to 200, with the change in value being in relation to the flow regime, after 100 iterations. The convergence criteria of the solution were defined in relation to the viscosity model. The common criterion for the convergence of the solutions was set to 10^{-5} and was related to the residuals of the numerical solutions of the continuity equations, the velocity and energy components. An additional condition of convergence of the $k-\varepsilon$ turbulence model was 10^{-5} and related to the turbulent kinetic energy k and the dissipation rate ε. Another additional criterion referred to the percentage deviation of the monitored drag aerodynamic coefficient value under axisymmetric flow.

3. Results and analysis of the semi-empirical calculation

In Table 3 are presented the results of a semi-empirical calculation according to the given Mach numbers under axisymmetric flow i.e., at zero-yaw, containing the total drag coefficient C_{D0} and its components C_{D1}, C_{D3}, C_{D4}, C_{Db} and C_{Df}, and also the depression ratio p_d/p_∞ behind the projectile , i.e., the projectile base pressure and the free air stream pressure.

M_a	C_{D0}	C_{D1}	C_{D3}	C_{D4}	C_{Db}	C_{Df}	p_d/p_∞
0,5	0,120	0,000	0,000	0,000	0,091	0,029	0,979
0,6	0,122	0,000	0,000	0,000	0,094	0,028	0,969
0,7	0,125	0,000	0,000	0,000	0,098	0,027	0,955
0,8	0,129	0,000	0,000	0,001	0,102	0,026	0,939
0,9	0,144	0,005	0,004	0,004	0,106	0,025	0,92
0,95	0,194	0,038	0,017	0,008	0,108	0,024	0,91
1	0,332	0,066	0,092	0,010	0,141	0,024	0,869
1,1	0,392	0,164	0,057	0,009	0,140	0,023	0,844
1,2	0,384	0,160	0,056	0,008	0,137	0,023	0,817
1,5	0,351	0,143	0,051	0,007	0,129	0,021	0,73
2	0,301	0,129	0,036	0,005	0,112	0,019	0,585
2,5	0,263	0,121	0,028	0,005	0,093	0,017	0,462
3	0,233	0,115	0,022	0,005	0,076	0,015	0,368

Table 3. Semi-empirical calculation results

Fig.6 shows the values of the total drag coefficient C_{D0} as a function of the Mach number M_a, obtained by semi-empirical calculation AERODR and that obtained experimentally available in (McCoy. 1998); where the two results have the same form of variation, almost steady at subsonic followed by a large peak at transonic and then a constant decrease at supersonic.

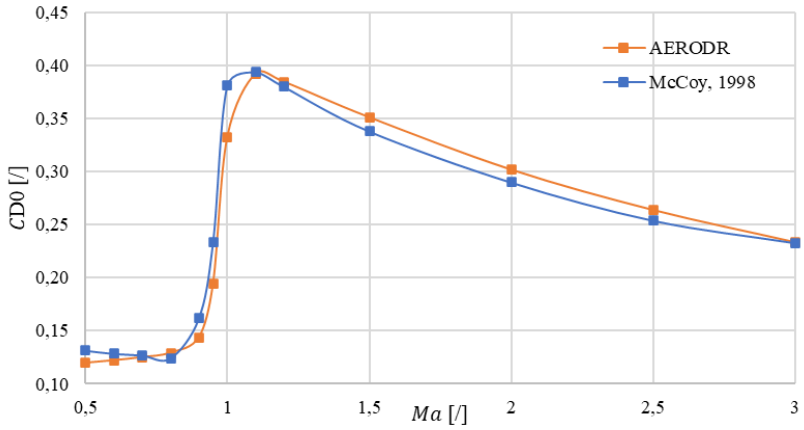

Fig. 6. Total drag coefficient C_{D0} as a function of M_a using semi-empirical approach

Fig.7 shows the values of the total drag coefficient C_{D0} under axisymmetric flow depending on the Mach number M_a, with its components C_{D1}, C_{D3}, C_{D4}, C_{Db} and C_{Df}, obtained by semi-empirical calculation AERODR; where the results have the same variation form as in the previous fig.6, except of those of C_{D4} and C_{Df} which are almost constant.

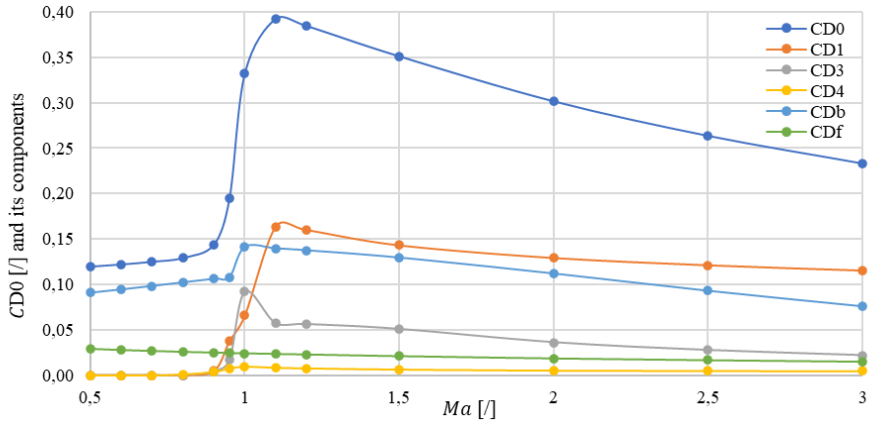

Fig. 7. Total drag coefficient C_{D0} and its components in the function of M_a using semi-empirical approach

Fig.8 shows the values of the depression ratio p_d/p_∞ behind the projectile depending on the Mach number M_a, obtained by semi-empirical calculation; where this ratio continually decreases especially in the supersonic regime, which means that the depression behind the bottom of the projectile has a greater influence in the supersonic than the subsonic and transonic.

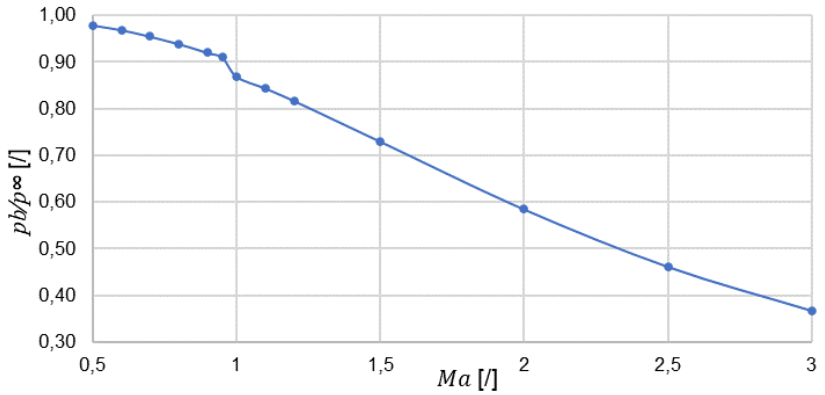

Fig. 8. Depression ratio p_d / p_∞ as a function of M_a using semi-empirical approach

Table 4 presents the deviation of the semi-empirical calculation results of the total drag coefficient C_{D0} in comparison with the experimental results (McCoy. 1998).

Flow regime	M_a	C_{D0} (experiment)	C_{D0} (semi-empirical)	Deviation %	Deviation % by flow regime
Subsonic	0,5	0,132	0,120	9,23	5,42
	0,6	0,129	0,122	5,26	
	0,7	0,127	0,125	1,76	
Transonic	0,8	0,124	0,129	3,76	7,64
	0,9	0,162	0,144	11,29	
	0,95	0,233	0,194	16,57	
	1	0,381	0,332	12,68	
	1,1	0,393	0,392	0,33	
	1,2	0,380	0,384	1,19	
Supersonic	1,5	0,338	0,351	3,82	2,91
	2	0,290	0,301	3,99	
	2,5	0,254	0,263	3,75	
	3	0,233	0,233	0,08	
In total					5.67

Table 4. Deviation of the semi-empirical calculation results from the experiment (McCoy. 1998)

From table 4 it can be seen that the C_{D0} values in transonic regime have a significant deviation from the reference values (McCoy. 1998), especially when the Mach number takes values between 0.9 and 1. In this flow regime, air circulates around the projectile at both transonic and supersonic velocities, which limits semi-empirical formulations to accurately predict C_{D0}. As for the value of C_{D0} in two subsonic and supersonic regimes, their deviations are acceptable, especially those in the supersonic regime where its average deviation does not exceed 3%.

Table 5 shows the values of the pressure drag coefficient C_{Dp}, the base drag coefficient C_{Db} and the friction drag coefficient C_{Df} as well as their influence rates of on the total drag coefficient C_{D0}. The pressure drag coefficient C_{Dp} is a consequence of the normal pressure on the projectile

surface, due to the appearance of shock waves; and is calculated by summing C_{D1}, C_{D3} and C_{D4}. In AERODR semi-empirical formulations, C_{Db} is calculated only in transonic and supersonic regimes; its effect in the subsonic regime is negligible compared to the effects of base and friction drags; therefore, in table 5, their values in this regime are equal to zero.

Flow regime	M_a	C_{D0}	C_{Dp}	$C_{Dp}/C_{D0}(\%)$	C_{Db}	$C_{Db}/C_{D0}(\%)$	C_{Df}	$C_{Df}/C_{D0}(\%)$
Subsonic	0,5	0,120	0,000	0,00	0,091	75,98	0,029	24,02
	0,6	0,122	0,000	0,00	0,094	77,44	0,028	22,56
	0,7	0,125	0,000	0,16	0,098	78,62	0,027	21,22
Transonic	0,8	0,129	0,001	0,93	0,102	79,23	0,026	19,85
	0,9	0,144	0,013	8,91	0,106	73,83	0,025	17,26
	0,95	0,194	0,062	31,84	0,108	55,56	0,024	12,55
	1	0,332	0,167	50,27	0,141	42,51	0,024	7,25
	1,1	0,392	0,229	58,43	0,140	35,58	0,023	5,97
	1,2	0,384	0,224	58,28	0,137	35,76	0,023	5,93
Supersonic	1,5	0,351	0,200	57,13	0,129	36,89	0,021	6,02
	2	0,301	0,171	56,67	0,112	37,13	0,019	6,21
	2,5	0,263	0,154	58,31	0,093	35,27	0,017	6,38
	3	0,233	0,142	60,94	0,076	32,53	0,015	6,52
Subsonic				0,05		77,35		22,60
Transonic				34,78		53,74		11,47
Supersonic				58,27		35,45		6,28
In total				33,99		53,56		12,44

Table 5. Influence of C_{Dp}, C_{Db} and C_{Df} on C_{D0} (semi-empirical approach)

From table 5 it can be seen that the influence of the pressure drag coefficient C_{Dp} is proportional to variations in M_a, i.e., to the flow velocity; on the other hand, the influence of the two coefficients, the base drag coefficient C_{Db} and the friction drag coefficient C_{Df}, is inversely proportional. The base drag coefficient C_{Db} is the most influential on the total drag coefficient C_{D0} in the subsonic and transonic regimes. As for the supersonic regime, the most influential coefficient is the pressure drag coefficient C_{Dp} with 58% of C_{D0}. The dominance of the base drag coefficient C_{Db} is more significant in the subsonic regime, where more than 75% of the total drag is of a vortex nature (the influence of pressure drag is negligible in that regime), while its influence in relation to the total drag in the supersonic regime decreases with the increase of the influence of pressure drag. This influence represents 54% of the total drag in all three flow regimes. The friction drag C_{Df} is a consequence of air viscosity and is higher if the surface obstructed by the flow is larger. The greatest impact of friction occurs in the subsonic regime. That influence is still significant, but in relation to other drag natures, it decreases, due to the appearance of pressure drag, in the transonic and further in the supersonic regime.

3. Results and analysis of the numerical calculation

A 2D axisymmetric numerical flow simulation was performed by Ansys Fluent for the 155mm M107 axisymmetric projectile, for different Mach numbers (from 0.5 to 3) using the boundary conditions presented above, while the reference area and reference length had values of $S = 0.01887 m^2$ and $d = 0.155 m$; where the $k-\varepsilon$ realizable model was used and the obtained results were compared with the experimental results (McCoy. 1998).

The numerical calculation results are shown in table 6; which differ from the semi-empirical results by the coefficient C_{D2}, which represents the pressure drag coefficient of the cylindrical part of the projectile. Its influence is almost negligible on the total drag; therefore, it is not taken into account in the AERODR semi-empirical calculation.

M_a	C_{D0}	C_{D1}	C_{D3}	C_{D4}	C_{D2}	C_{Db}	C_{Df}	p_d/p_∞
0,5	0,127	-0,004	0,028	0,018	0,001	0,030	0,054	0,995
0,6	0,126	-0,004	0,029	0,020	0,001	0,029	0,051	0,993
0,7	0,128	-0,004	0,031	0,023	0,001	0,028	0,049	0,990
0,8	0,127	-0,003	0,032	0,028	0,001	0,023	0,046	0,990
0,9	0,170	0,010	0,054	0,046	0,003	0,011	0,044	0,996
0,95	0,227	0,030	0,084	0,042	0,004	0,022	0,044	0,986
1	0,381	0,075	0,097	0,038	0,004	0,124	0,044	0,890
1,1	0,392	0,127	0,076	0,033	0,003	0,110	0,043	0,884
1,2	0,377	0,128	0,065	0,030	0,002	0,109	0,042	0,863
1,5	0,337	0,121	0,046	0,023	0,002	0,104	0,041	0,797
2	0,291	0,115	0,031	0,016	0,001	0,088	0,040	0,695
2,5	0,253	0,108	0,022	0,012	0,001	0,072	0,038	0,604
3	0,223	0,103	0,017	0,008	0,000	0,059	0,036	0,530

Table 6. Numerical calculation results

Fig.9 shows the values of the total drag coefficient C_{D0} as a function of the Mach number M_a, obtained by numerical calculation and that obtained experimentally available in (McCoy. 1998); where the two curves have identical forms of variation.

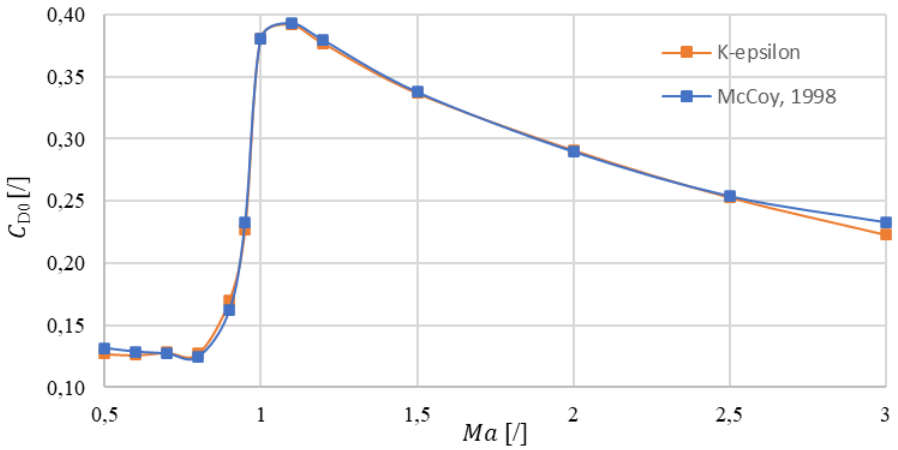

Fig. 9. Total drag coefficient C_{D0} as a function of M_a using numerical simulations

Fig.10 shows the values of the total drag coefficient C_{D0} under axisymmetric flow depending on the Mach number M_a, with its components C_{D1}, C_{D3}, C_{D4}, C_{D2}, C_{Db} and C_{Df}, obtained by numerical calculation; where the results have the same form of variation as in the previous fig.9, except for the variation in C_{D2} and C_{Df} which are almost constant and the variation in C_{Db} in the transonic regime which has a small decrease followed by a large peak.

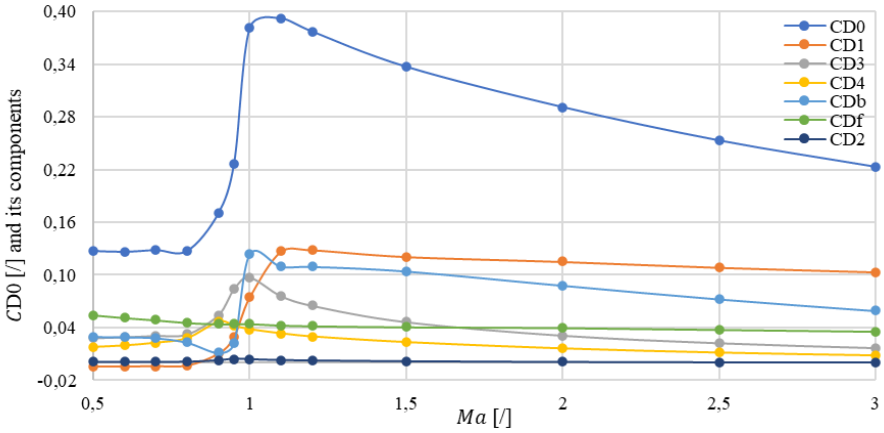

Fig. 10. Total drag coefficient C_{D0} and its components in the function of M_a using numerical simulations

Fig.11 presents the values of the depression ratio p_d/p_∞ behind the projectile depending on the Mach number M_a, obtained by numerical calculation; where this ratio is almost constant in the subsonic regime and part of the transonic regime, up to Mach number 0.9; followed by a sudden decrease in the second part of transonic regime and then a permanent decrease in the supersonic regime, which means that the depression behind the bottom of the projectile has a greater influence in the latter regime.

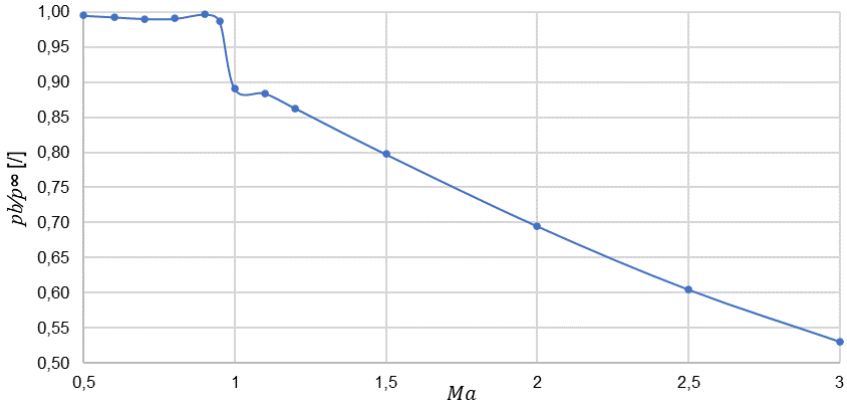

Fig. 11. Depression ratio p_d/p_∞ as a function of M_a using numerical simulations

In fig.12 is presented the flow Mach number profile obtained for different values of Mach number at zero-yaw.

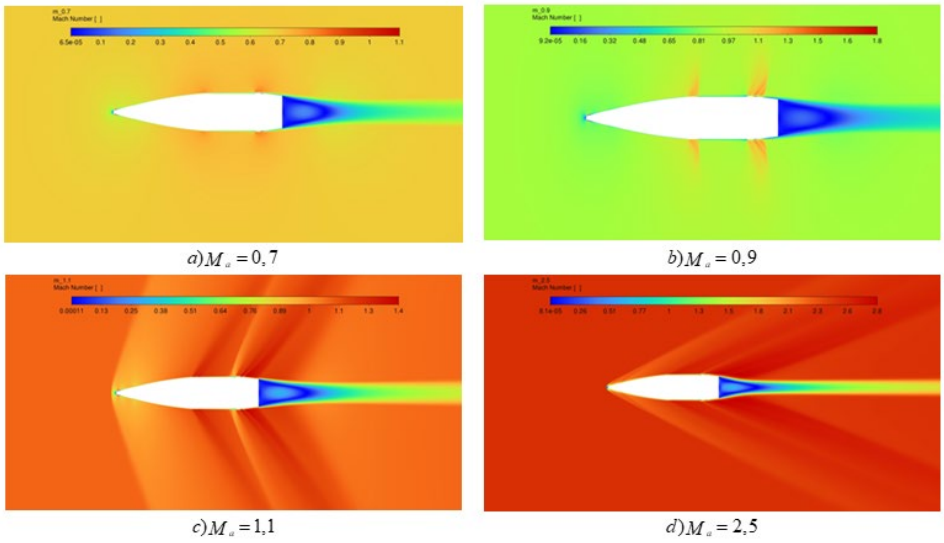

$a) M_a = 0,7$ $b) M_a = 0,9$

$c) M_a = 1,1$ $d) M_a = 2,5$

Fig. 12. Mach number profile at zero-yaw

Fig.13 presents the obtained profile of the static pressure of the flow for different values of the Mach number at zero-yaw.

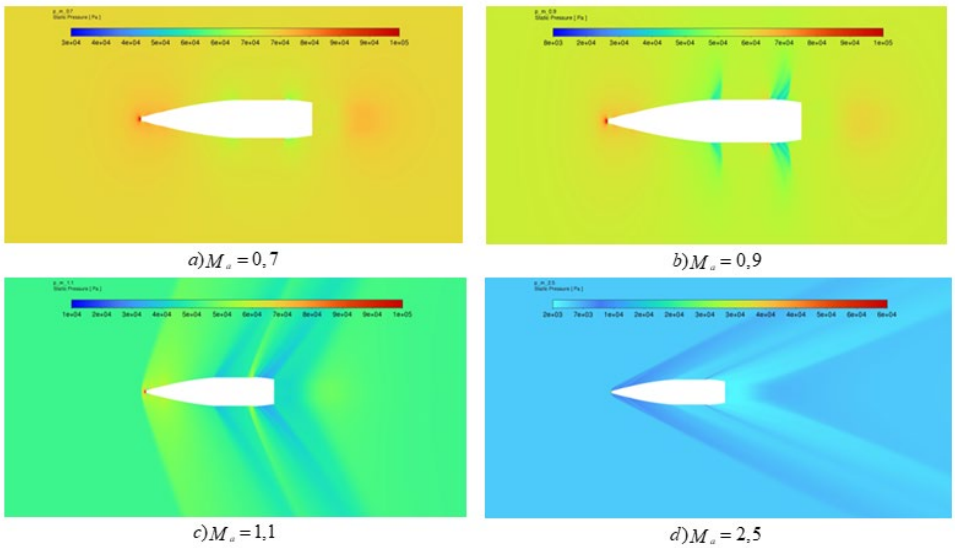

$a) M_a = 0,7$ $b) M_a = 0,9$

$c) M_a = 1,1$ $d) M_a = 2,5$

Fig. 13. Static pressure profile at zero-yaw

Fig.14 shows the resulting flow velocity vector in the base zone behind the projectile for different Mach number values at zero-yaw.

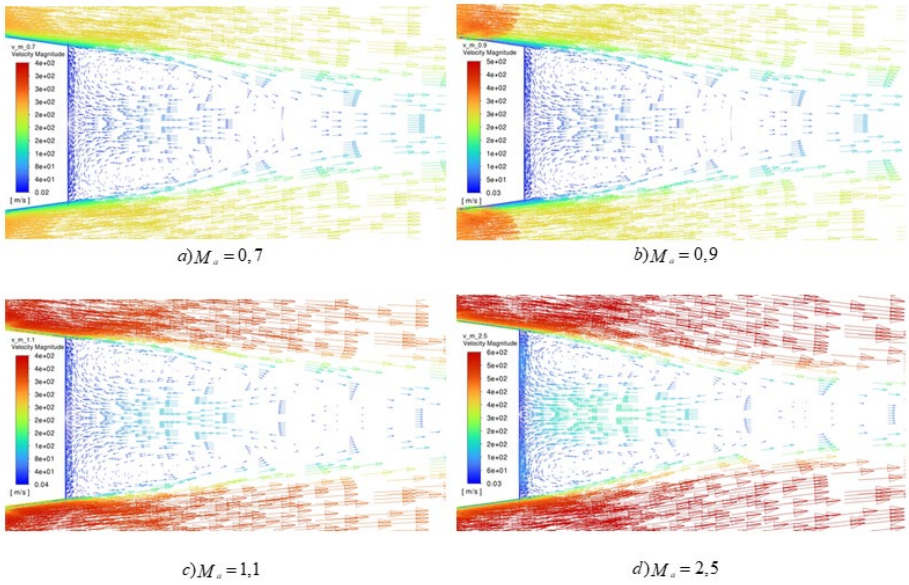

Fig. 14. Flow velocity vector in the base zone at zero-yaw

From fig.12 and fig.13 it is noted the appearance of phenomena which characterize the transonic regime and mainly the supersonic regime, such as the normal and oblique shock waves and the Mach cone as the limit of the flow disturbed, which leads to an increase in the influence of pressure drag on the total drag. Fig.14 shows the formation of two large symmetrical zones of backflow behind the projectile, where their dimensions increase with higher values of the Mach number. During the projectile flight, the backflow was directly generated behind the base due to the large angle of deflection behind it. This causes separation and the formation of backflow known as the recirculation region which leads to an increase in vortex drag (base drag).

Flow regime	M_a	C_{D0} (experiment)	C_{D0} (numerical calculation)	Deviation %	Deviation % by flow regime
Subsonic	0,5	0,132	0,127	3,529	2,09
	0,6	0,129	0,126	2,068	
	0,7	0,127	0,128	0,674	
Transonic	0,8	0,124	0,127	2,150	1,80
	0,9	0,162	0,170	4,938	
	0,95	0,233	0,227	2,575	
	1	0,381	0,381	0,086	
	1,1	0,393	0,392	0,356	
	1,2	0,380	0,377	0,707	
Supersonic	1,5	0,338	0,337	0,264	1,31
	2	0,290	0,291	0,406	
	2,5	0,254	0,253	0,350	
	3	0,233	0,223	4,214	
In total					1.72

Table 7. Deviation of the numerical calculation results from the experiment (McCoy. 1998)

Table 7 presents the deviation of the numerical calculation results of the total drag coefficient C_{D0} in comparison with the experimental results (McCoy. 1998).

According to table 7 the values of C_{D0} have a small deviation from the reference values (McCoy. 1998), where the greatest deviation by Mach number does not exceed 5% and by the flow regime is almost 2%. This confirms that the numerical approach used in this work gave very acceptable results and very close to the experiment with the use of the $k-\varepsilon$ realizable model.

Table 8 shows the values of the pressure drag coefficient C_{Dp}, the base drag coefficient C_{Db} and the friction drag coefficient C_{Df} as well as their influence rates of on the total drag coefficient C_{D0}, recalling that C_{Dp} is the sum of C_{D1}, C_{D3}, C_{D4} and C_{D2}.

Flow regime	M_a	C_{D0}	C_{Dp}	C_{Dp}/C_{D0} (%)	C_{Db}	C_{Db}/C_{D0} (%)	C_{Df}	C_{Df}/C_{D0} (%)
Subsonic	0,5	0,127	0,043	33,69	0,030	23,46	0,054	42,91
	0,6	0,126	0,046	36,30	0,029	23,26	0,051	40,75
	0,7	0,128	0,051	39,55	0,028	22,16	0,049	38,09
Transonic	0,8	0,127	0,058	45,99	0,023	18,33	0,046	35,99
	0,9	0,170	0,114	67,08	0,011	6,71	0,044	25,98
	0,95	0,227	0,160	70,46	0,022	9,85	0,044	19,49
	1	0,381	0,213	56,02	0,124	32,44	0,044	11,66
	1,1	0,392	0,239	61,03	0,110	27,94	0,043	10,91
	1,2	0,377	0,226	59,88	0,109	29,03	0,042	11,14
Supersonic	1,5	0,337	0,192	57,09	0,104	30,92	0,041	12,11
	2	0,291	0,163	56,18	0,088	30,25	0,040	13,70
	2,5	0,253	0,143	56,58	0,072	28,64	0,038	14,95
	3	0,223	0,129	57,82	0,059	26,57	0,036	16,01
Subsonic				36,52		22,96		40,58
Transonic				60,08		20,72		19,20
Supersonic				56,92		29,10		14,19
In total				53,67		23,81		22,59

Table 8. Influence of C_{Dp}, C_{Db} and C_{Df} on C_{D0} (numerical simulations)

From table 8 it can be seen that the influence of the pressure drag coefficient C_{Dp} on C_{D0} is proportional to variations in the Mach number, up to $M_a = 0,95$ which corresponds to a maximum influence rate of 70%; as to the remaining Mach number interval (from 1 to 3); it takes more or less identical impact rates, close to 57%. On the other hand, the influence of the two coefficients of the base drag C_{Db} and of the friction drag C_{Df} on C_{D0} is inversely proportional to the C_{Dp} variations where their influences are important in the subsonic regime, then they assume minimum levels of influence at certain values of the Mach number in the transonic regime, then in the same flow regime they continue their influences on the total drag with influence rates lower than that of pressure drag C_{Dp}. The pressure drag C_{Dp} is the most influential on the total drag C_{D0} in the transonic and supersonic regimes. As for the subsonic regime, the friction drag C_{Df} is the most influential with 40% of C_{D0}.

The dominance of the pressure drag coefficient C_{Dp} is more significant in both the transonic and supersonic regimes, where about 60% of the total drag is of a shock wave nature; while its influence in relation to the total drag in the subsonic regime is almost equal to the influence of the friction drag which is the most influential in this flow regime. That influence is still

significant, but in relation to the pressure drag it decreases in the transonic and further in the supersonic regime. As for the base drag C_{Db} it has a significant influence on the total drag, but contrary to the results of the semi-empirical calculation, it is not dominant with influence rates which take 23% in the subsonic regime, 21% in the transonic regime, 29% in the supersonic regime and 24% in all three flow regimes. The difference in base drag influence rate between numerical calculation and semi-empirical calculation in all three flow regimes can be justified by the fact that CFD simulations are based on the numerical solution of fundamental equations of fluid dynamics, such as the Navier-Stokes equations, which are mathematical representations of the laws of conservation of mass, momentum and energy in a fluid. On the other hand, semi-empirical methods often rely on simplified models and empirical approximations, which can lead to different results; however, these methods are faster and less expensive in terms of computational resources.

4. Conclusion

During movement in the air and due to the interaction of the axisymmetric projectile and the air, a total aerodynamic force and moment occur. The resultant force is composed into drag, side, and lift forces, and the resultant moment into roll moment, pitch moment and yaw moment. The predictive calculation of the drag force is an inevitable approach in external ballistics where this force is the only force that opposes the movement of the projectile in an axisymmetric flow at zero-yaw. Hence the main objective of the work was, on the one hand, the semi-empirical and numerical prediction of the total drag coefficient C_{D0} for of the 155mm M107 axisymmetric projectile; on the other hand, the analysis of the influence of each drag type on the total drag.

According to the results of the semi-empirical calculation presented in this work, it can be seen that the C_{D0} values show a significant deviation from the reference values (McCoy. 1998), especially in the transonic regime (Mach number between 0.9 and 1). The same results also show that the base drag coefficient C_{Db} is more influential in the two regimes, subsonic and supersonic. concerning its influence in the supersonic regime on to the total drag, it decreases with the increase of the influence of the pressure drag C_{Dp} (58% of the total drag in this regime). As for friction drag C_{Df}, its influence is significant in the subsonic region.

From the results of the numerical calculation presented in this work, it was shown that the numerical approach used in this work gave values of the total drag coefficient C_{D0} almost identical to the reference results (McCoy. 1998) with the use of the $k-\varepsilon$ realizable model, since the largest deviation according to the Mach number does not exceed 5% and according to the flow regime is almost 2%. As for the influence of drag types on the total drag, it was found from the same results that the pressure drag C_{Dp} is the most influential on the total drag in the transonic and supersonic regimes. As for the subsonic regime, C_{Df} is the most dominant with 40% of the total drag. For the base drag C_{Db}, its influence rates were 23% in the subsonic regime, 21% in the transonic regime and 29% in the supersonic regime. The numerical simulation of the flow carried out in this work made it possible to simulate the appearance of phenomena such as normal and oblique shock waves and the Mach cone as the limit of the disturbed flow. It also provided a good representation of the process of formation of two large symmetrical zones of backflow behind the projectile called the recirculation region which grow larger with higher Mach number values.

This work may have future prospects which may relate to the reduction of the total drag C_{D0} of the projectile by reducing the influence of one of its components, such as on the one hand

examining the optimal geometric shape of the projectile in order to reduce the pressure drag C_{Dp}, on the other hand change the shape of the bottom of the projectile (base shape) or add a gas generator (base bleed), which makes it possible to reduce the base drag C_{Db}.

References

Aziz, M., Ibrahim, A., Ahmed, M., & Riad, A. (2020). Multi-fidelity drag prediction for base bleed projectile. IOP Conference Series Materials Science and Engineering.

Belaidouni, H., Živković, S., & Samardžić, M. (2016). Numerical Simulations in Obtaining Drag Reduction for Projectile with Base Bleed. Scientific Technical Review, 66(2), 36-42.

Chang, S., & Li, D. (2023). Aerodynamic Coefficients of a Microspoiler for Spin-Stabilized Projectiles. Journal of spacecraft and rockets.

Dali, M., & Jaramaz, S. (2019). Optimization of Artillery Projectiles Base Drag Reduction Using Hot Base Flow. Thermal Science, 23(1), 353-364.

DeSpirito, J. (2017). CFD Aerodynamic Characterization of 155-mm Projectile at High Angles-of-Attack. 35th AIAA Applied Aerodynamics Conference.

Fonte-Boa, R., Borges, J., & Chaves, J. (2017). AnAlysis of externAl bAllistics for A projectile of cAliber 155 mm. Proelium, 7(12), 227 - 241.

McCoy, R. (1981). "MC DRAG" - a comptuter program for estimating the drag coefficients of projectiles. Maryland: Ballistic Research laboratory.

McCoy, R. L. (1998). Modern Exterior Ballistics. 4thedition, ISBN-0-7643-0720-7, Schiffir Publishing Ltd.

Nicolás-Pérez, F., Velasco, F., García-Cascales, J., Otón-Martínez, R., López-Belchí, A., Moratilla, D., Laso, A. (2017). On the accuracy of RANS, DES and LES turbulence models for predicting drag reduction with Base Bleed technology. Aerospace Science and Technology, 67, 126-140.

Paul, S., Vinoth Raj, A., & Senthil Kumar, C. (2023). Inward turning base-bleed technique for base drag reduction. The Aeronautical Journal, 127, 370–397.

Regodić, D. (2003). Zbirka rešenjih zadataka iz spoljne balistike. Beograd: Vojna Akademija.

Regodić, D. (2006). Spoljna balistika. Beograd: Vojna akademija.

Regodić, D., Jevremovic, A., & Jerković, D. (2013). The prediction of axial aerodynamic coefficient reduction using base bleed. Aerospace Science and Technology, 31, 24-29.

Roy, A. (2012). A First Course on Aerodynamics. Ventus Publishing ApS.

Sahu, J., & Heavey, K. (1997). Numerical Investigation of Supersonic Base Flow with Base Bleed. JOURNAL OF SPACECRAFT AND ROCKETS 34 (1), 62-69. doi:10.2514/2.3173

Serdarevic-Kadic, S., & Terzic, J. (2019). Effects of Base Shape to Drag at Transonic and Supersonic Speeds by CFD. DAAAM International Scientific, 071-080.

Sivasubramanian, J., Sandberg, R., von Terzi, D., & Fasel, H. (2006). Numerical Investigation of Flow Control Mechanisms for Drag Reduction in Supersonic Base-Flows. 44th AIAA Aerospace Sciences Meeting and Exhibit. doi:10.2514/6.2006-902

Szklarski, A., Gł˛ebocki, R., & Jacewicz, M. (2020). Impact point prediction guidance parametric study for 155 mm rocket assisted artillery projectile with lateral thrusters. Archive of mechanical engineering, 67(1), 31-56.

Torangatti, K., & Dr. Basawaraj. (2014). Drag prediction and validation of standard m549, 155mm projectile. International Journal of Engineering Research and Reviews, 2(3), 26-32.

Viličić, J., & Gajić, M. (1979). Balistika.